Global increase in tropical cyclone outflow height

Zhihao Feng,[1,6] Yuan Sun,[2,6,*] Wei Zhong,[2,*] Haikun Zhao,[3,*] Weimin Zhang,[1] Yanning Liang,[1] Yanluan Lin,[4] and Zongbao Bai[5]

*Correspondence: sunyuan1214@126.com (Y.S.); zhongwei@nudt.edu.cn (W.Z.); haikunzhao@nuist.edu.cn (H.Z.)

Received: March 2, 2026; Accepted: July 10, 2026; Published Online: July 14, 2026; https://doi.org/10.59717/j.xinn-geo.2026.100248

GRAPHICAL ABSTRACT

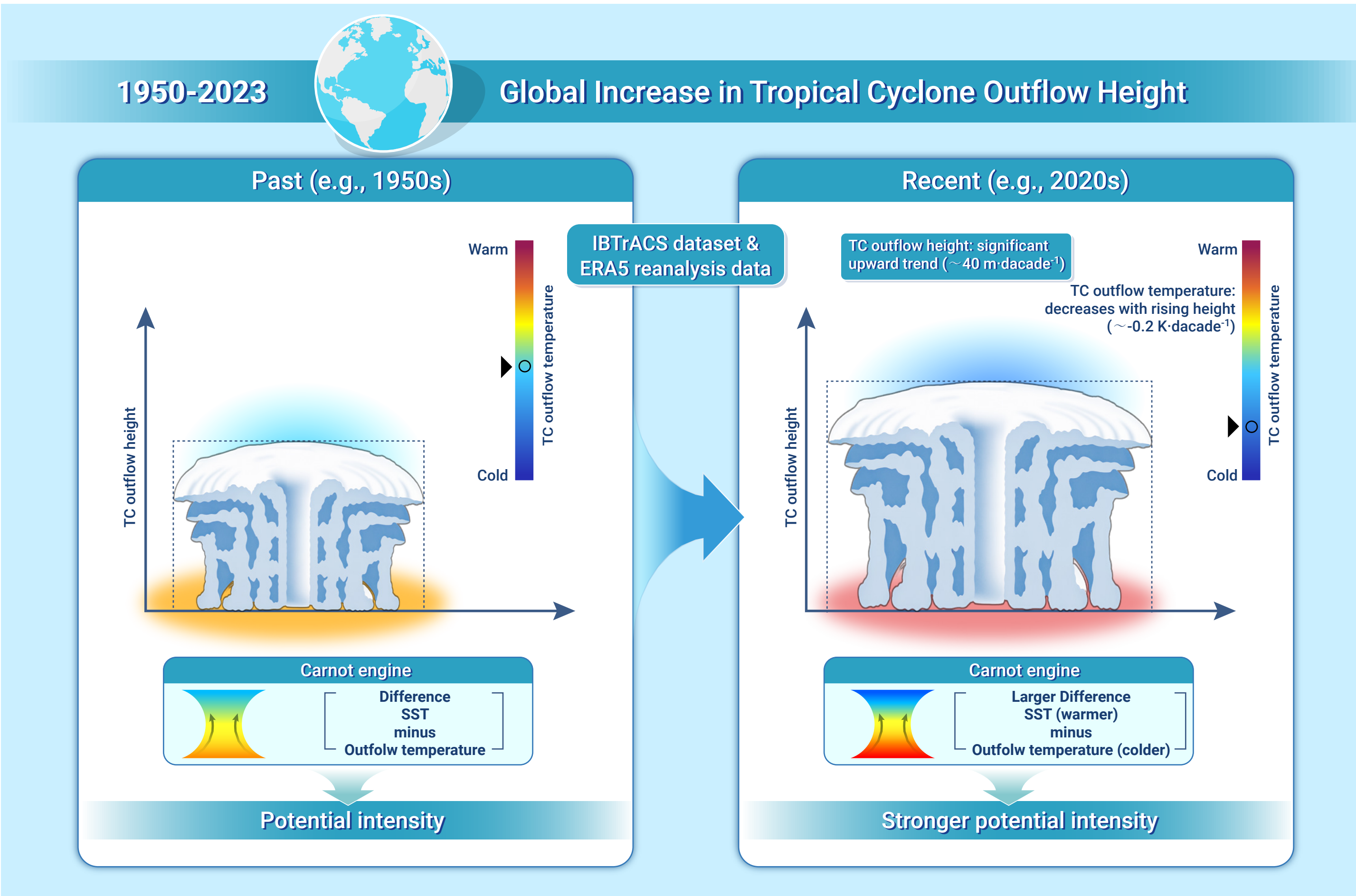

PUBLIC SUMMARY

- Global tropical cyclone (TC) outflow height has risen significantly over 74 years.
- Anthropogenic forcing, not natural variability, is the primary cause of increasing TC outflow height.
- Rising outflow height cools the outflow layer, indirectly enhancing TC potential intensity under warming.

Global increase in tropical cyclone outflow height

Zhihao Feng,[1,6] Yuan Sun,[2,6,*] Wei Zhong,[2,*] Haikun Zhao,[3,*] Weimin Zhang,[1] Yanning Liang,[1] Yanluan Lin,[4] and Zongbao Bai[5]

[1]College of Meteorology and Oceanography, National University of Defense Technology, Changsha 410073, China
[2]College of Advanced Interdisciplinary Studies, National University of Defense Technology, Nanjing 211100, China
[3]State Key Laboratory of Climate System Prediction and Risk Management/Key Laboratory of Meteorological Disaster, Ministry of Education/Collaborative Innovation Center on Forecast and Evaluation of Meteorological Disasters, Nanjing University of Information Science and Technology, Nanjing 210044, China
[4]Ministry of Education Key Laboratory for Earth System Modeling, Department of Earth System Science, Tsinghua University, Beijing 100084, China
[5]Department of Navigation, Dalian Naval Academy, Dalian 116000, China
[6]These authors contributed equally
*Correspondence: sunyuan1214@126.com (Y.S.); zhongwei@nudt.edu.cn (W.Z.); haikunzhao@nuist.edu.cn (H.Z.)

Received: March 2, 2026; Accepted: July 10, 2026; Published Online: July 14, 2026; https://doi.org/10.59717/j.xinn-geo.2026.100248

Citation: Feng Z., Sun Y., Zhong W., et al. (2026). Global increase in tropical cyclone outflow height. *The Innovation Geoscience* **4**:100248.

Compared to air–sea interactions, relatively little is known about the impact of global warming on tropical cyclone (TC) outflow environment, even though it makes an important contribution to TC intensity. Here we present a global trend analysis of TC outflow height for 1950–2023 based on the IBTrACS and ERA5 data. TC outflow height has increased globally by 40.29 ± 8.28 m·decade^{-1}, and all six basins exhibit notable upward trends beyond natural variability, likely due to global warming. The increase in TC outflow height leads to decreased outflow temperature (-0.21 ± 0.08 K·decade^{-1}), thereby indirectly enhancing TC potential intensity (PI). The contributions of TC outflow environment change to TC PI variations were quantitatively assessed. Under global warming, TC outflow height is expected to continue increasing, potentially leading to significant changes in TC outflow environment and ultimately driving an increase in future TC intensity.

INTRODUCTION

The relationship between global warming and tropical cyclone (TC) activity, along with the associated disasters, is widely studied.[1,2] In recent decades there has been a significant increase in sea surface temperature (SST),[3] with concurrent changes in atmospheric circulation patterns including expansion of the tropics.[4,5] Such changes in oceanic and atmospheric environments are believed to influence TC intensity.[6] Theory [7] and numerical simulations [8] both suggest that global warming will cause an increase in TC intensity and strong TC frequency globally. However, the detection of long-term trend in TC intensity has been a subject of considerable debate, depending in part on details of the intervention of natural variability,[9] adjustments for storm undercounts or intensity biases.[10] To shed light on the possible long-term trend in TC intensity, it is necessary to investigate the observed trend of the factors contributing to TC intensity in the past.

Emanuel (1986) developed the Potential Intensity (PI) theory, which has been widely adopted in TC research.[11] By treating a TC as a Carnot heat engine, the maximum sustained wind speed is thermodynamically constrained by the temperature difference between the heat source (SST) and the heat sink (TC outflow temperature). However, compared to studies on TC air–sea interaction,[12] relatively few investigations have focused on the TC outflow environment, despite its important influence on TC potential intensity. Emanuel et al. (2013) identified a notable decreasing trend in tropical tropopause layer (TTL) temperature over the North Atlantic, which may contribute to an increase in PI.[13] Nevertheless, Wing et al. (2015) argued that this cooling trend is confined to the North Atlantic basin and is not statistically significant in other ocean basins, suggesting it should not be considered a global phenomenon.[14] Subsequently, a study employed numerical modeling to confirm the enhancing effect of TTL cooling on TC intensity.[15] Nevertheless, limited by the coarse resolution of earlier datasets, previous studies have primarily examined the impacts of large region TTL temperature variations on TC activity, which may not adequately represent the thermodynamic conditions near individual TCs. More importantly, TC outflow layer typically resides below the TTL and exhibits vertical variability within the 300–100 hPa.[16-18] Therefore, the TC outflow layer over a small area near TC cannot be equated with the regional averaged TTL. In addition, upper-atmosphere geopotential height is projected to increase in response to global warming.[19] How this upward shift modulates the outflow layer environment—particularly the vertical position of the TC outflow layer—and consequently affects global changes in PI remains poorly quantified.

In this study, datasets of the International Best Track Archive for Climate Stewardship (IBTrACS) for 1950–2023, and the European Centre for Medium-Range Weather Forecasts Reanalysis (ECMWF) Reanalysis v.5 (ERA5) were used to investigate changes in TC outflow possibly associated with global warming. Distinct from previous studies that analyze broad environmental fields, we focus specifically on the outflow environment within a 500 km radius of the TC center. Our findings indicate a statistically significant increase in TC outflow height and all basins have shown significant long-term upward trends. This upward trend in TC outflow height likely induces a corresponding reduction of outflow temperature, which would enhance the difference between the TC underlying SST and outflow layers and thus enhanced TC intensity. This study considers possible reasons for the observed trends in TC outflow height, and explores the relationship among TC outflow height, outflow temperature and intensity.

MATERIALS AND METHODS

IBTrACS dataset and ERA5 reanalysis data

The TC data used in this study include those for all numbered and unnumbered TCs recorded in the IBTrACS dataset for 1950–2023, resulting from reanalysis of storm position and intensity based on all available data including ship, surface, and satellite observations.[5,20] The IBTrACS dataset includes the latitude and longitude of TC centers, minimum sea-level pressure, and 2-minute averaged maximum wind speed. For the IBTrACS dataset, measurements taken near the time of LMI are subject to much smaller uncertainties.[4] Therefore, the accuracy of “LMI records” in this study is expected to be a little higher than that of “All records”.

The ERA5 reanalysis data is based on an extensive array of observational data from various sources including satellite telemetry, terrestrial meteorological stations, and radiosonde ascents, with detailed reconstruction of the atmospheric state based on numerical weather-prediction models.[21] In this study, latitude and longitude coordinates, wind speed, sea level pressure, geopotential height, humidity, and temperature derived from the ERA5 dataset were used to determine the characteristics of TC outflow layers, providing atmospheric data at a high spatial resolution of 0.25° with vertical stratification of 25 hPa over the period 1950–2023.

Three carbon emission scenarios based on CMIP6 Data

The CMIP6 refers to the sixth phase of the Coupled Model Intercomparison Project, and the use of CMIP6 data for global warming simulations has been widely recognized.[22] EC-Earth3, one among the CMIP6 models, performs well in TC simulations.[23] Therefore, we selected Historical, SSP245, and SSP585 experimental data from the EC-Earth3 model to establish three distinct carbon emission scenarios, which were used to examine the sensitivity of TC activity to global warming. Specifically, we used data from the historical scenario for the 1985–2014 period to construct the numerical model background for the historical carbon emission scenario and data from the SSP245 (SSP585) scenario for the 2071–2100 period to construct the background for the medium (high)-carbon emission scenario.

TC position information determination

Here, TC positions were based on not only ERA5 but also IBTrACS data. The TC identification criteria in the ERA5 reanalysis data, based on minimum sea level pressure, maximum 10-meter wind speed, and other factors, are applied to the surface layer.[24] Additionally, the TC center in the outflow layer is re-identified based on the relationship between geopotential height and pressure,[25] in order to avoid mistakes caused by TC structure. TC numbers and positions sometimes differed between the datasets, e.g., some TCs in the IBTrACS (ERA5) dataset could not be found in the ERA5 (IBTrACS) dataset, and some TCs have shifts in their center locations between two datasets.[26] To address this issue, we matched ERA5 tracks to IBTrACS tracks, initially determining the latitude and longitude of TC centers using the latter, with adjustment based on ERA5 information if the mean spatial separation was < 5° over the corresponding paired track points.[27] If the spatial separation was > 5°, the TC was removed because it had not been recorded concurrently in both datasets. To ensure that TCs had the same lifetime in both datasets, those identified in the ERA5 dataset were truncated according to their lifecycle period in the IBTrACS dataset. This process may have resulted in the exclusion of some TCs. We then investigated TC outflow layers and their associated activities based on the revised TC position information.

TC outflow height and temperature

Previous studies have constrained TC outflow layer heights to within the range of 300–100 hPa.[17,18] Here, we calculated radial velocities across specified pressure layers, encompassing eight layers (300, 250, 225, 200, 175, 150, 125, and 100 hPa), within a 500 km radius of the revised TC center. The TC outflow layer is defined as the pressure layer exhibiting the maximum radial velocity within a 500 km radius of the TC center, expressed as:

$$P_{\text{outflow}} = P_i(\max(V_r)) \tag{1}$$

where P_{outflow} (hPa) is the TC outflow pressure layer, P_i is the range of pressure layers, and V_r (m·s^{-1}) is the mean TC radial velocity within a 500 km radius of the revised TC center.

Note that, to minimize the influence of environmental wind on the results, the average environmental field within a 500 km radius of the TC center was removed prior to calculating the radial velocity.[28] The percentages of each pressure layer in the TC outflow layer are illustrated in Figure S1.

TC outflow height (TC outflow temperature) is defined as the mean geopotential height (temperature) within a 500 km radius of revised TC center in the outflow layer. The calculation can be expressed as follows:

$$H_{\text{outflow}} = \frac{1}{A}\sum_{i=1}^{N} H_i(P_{\text{outflow}})S_i \tag{2}$$

$$T_{\text{outflow}} = \frac{1}{A}\sum_{i=1}^{N} T_i(P_{\text{outflow}})S_i \tag{3}$$

where H_{outflow} (m) is the TC outflow height, T_{outflow} (K) is the TC outflow temperature, A (km^2) is the area within a 500 km radius of TC center, N is the number of meshed grids in ERA5 dataset with a spatial resolution of 0.25°×0.25° in A area, $H_i(P_{\text{outflow}})$ (m) is the geopotential height at i gridpoint in P_{outflow} layer, $T_i(P_{\text{outflow}})$ (K) is the temperature at i gridpoint in P_{outflow} layer, and S_i (km^2) represents the area of i gridpoint, namely the area of 0.25° × 0.25°.

Basin differences and natural variability

We considered the regional variability of TC outflow height upward trends and delineated TC activity regions to six basins: the Northwest Pacific (NWP), Northeast Pacific (NEP), South Pacific (SP), North Atlantic (NA), North Indian Ocean (NIO), and South Indian Ocean (SIO) (Figure 1).[29]

Natural variability is important in studies of long-term changes in TC activity, and we evaluated the effect of natural variability on the uptrend in TC outflow height by removing it from TC outflow height time series.[4] The predominant influence of natural variability differs across basins, and for each basin natural variability indices were considered as follows: the El Niño–Southern Oscillation (ENSO), Pacific Decadal Oscillation (PDO), and Interdecadal Pacific Oscillation (IPO) in the NWP[30] and NEP;[31] the ENSO in the SP;[32] the Atlantic Multi-decadal Oscillation (AMO) and the North Atlantic Oscillation (NAO) in the NA;[33,34] the ENSO and the Indian Ocean Dipole (IOD) in the NIO; [35-37] and the Antarctic Oscillation (AAO) in the SIO.[38]

Factors contributing to changes in TC outflow temperature

We attributed the change in TC outflow temperature to two main factors: the increase in TC outflow height, and change in upper-atmosphere temperature. The contributions of these factors to TC outflow temperature were calculated globally, and separately for each basin, as follows:

$$\Delta T_{combine} = \Delta T_{height} + \Delta T_{upper\_atm} \tag{4}$$

$$E_{Pct} = \Delta T_{combine} / \Delta T_{outflow} \tag{5}$$

where ΔT_{height} (K) is the temperature change caused by TC outflow height increase, and ΔT_{upper_atm} (K) is the temperature change caused by the change of upper-atmosphere temperature, $\Delta T_{combine}$ (K) is the combined effects of ΔT_{height} and ΔT_{upper_atm}, $\Delta T_{outflow}$ (K) is the change in TC outflow temperature , E_{Pct} (%) is explainable percentage which indicated the explainability of combine effect.

In estimating the factor for TC outflow height change, we calculated the mean vertical temperature gradient within the outflow layers (300–100 hPa) with a vertical resolution of 25 hPa over the period 1950–2023 using the ERA5 dataset for the six basins. To quantify the impact of the increase in outflow height, we multiplied it by the vertical temperature gradient to obtain the temperature change:

$$\Delta T_{height} = \Delta H_{height} \cdot \frac{\partial T}{\partial H} \tag{6}$$

where ΔH_{height} (m) is the increase in TC outflow height from 1950 to 2023, and $\frac{\partial T}{\partial H}$ (K·m^{-1}) is the mean vertical temperature gradient within the outflow layers (300–100 hPa).

In estimating the factor for upper-atmosphere temperature change, we multiplied the temperature change from 1950 to 2023 within the 300–100 hPa layer (Figure S4) by the percentage of each pressure layer in the TC outflow height (Figure S1).

$$\Delta T_{upper\_atm} = \sum_{i=1}^{8} (\Delta T(P_i) \cdot Pct(P_i)) \tag{7}$$

where $\Delta T(P_i)$ (K) is the temperature change from 1950 to 2023 in each pressure layer (for a total of eight layers), and $Pct(P_i)$ (%) is the percentage of each pressure layer in the TC outflow height.

Tropical cyclone potential intensity (PI)

The PI, defined by Emanuel (1995) and improved by Bister and Emanuel (2002), can be calculated as follows:[39-41]

$$V_m^2 = \frac{C_k}{C_d}\frac{T_s}{T_0}(\text{CAPE}^* - \text{CAPE}^m) \tag{8}$$

where PI is defined as the low-level maximum wind speed of a TC (V_m), T_s is the SST, T_0 is the mean outflow temperature, C_k is the exchange coefficient for enthalpy, C_d is a drag coefficient, the convective available potential energy (CAPE) of a saturated parcel lifted from saturation at sea level is denoted as CAPE* (saturation CAPE), and the CAPE of a parcel with the environmental relative humidity, surface air temperature, and TC eyewall pressure is denoted as CAPE^m (radius of the maximum-wind CAPE).

The calculation of CAPE is affected by TC outflow temperature and TC underlying SST. The equation (6) can be written as:[41]

$$V_m^2 = c_p(T_s - T_0)\frac{T_s}{T_0}\frac{C_k}{C_d}(\ln\theta_e^* - \ln\theta_e)|_m \tag{9}$$

where θ_e^* the saturation equivalent potential temperature at the ocean surface, and θ_e the boundary layer equivalent potential temperature. The last factor in (7) is evaluated at the radius of maximum winds.

Factors contributing to changes in TC potential intensity

To calculate the contribution of TC outflow temperature and TC underlying

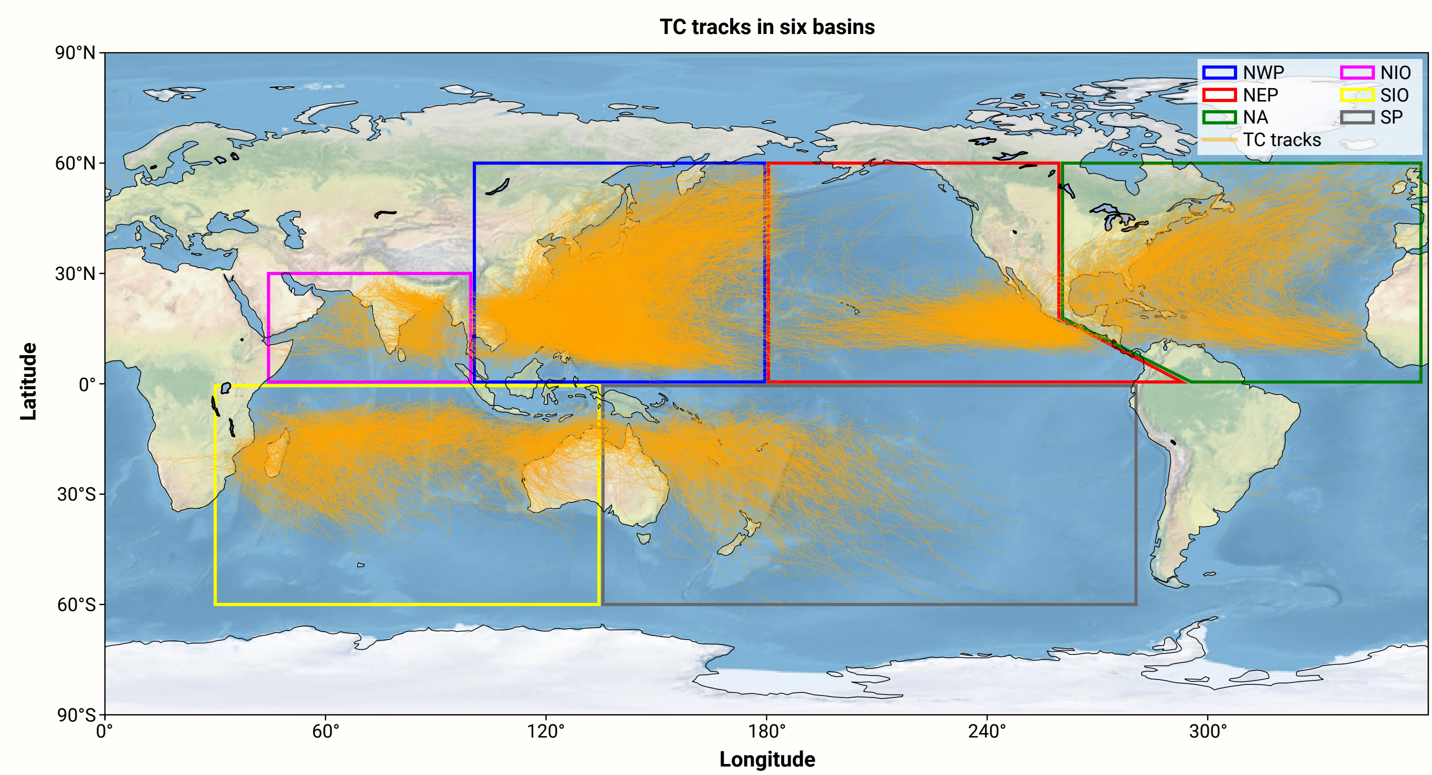

Figure 1. TC tracks in the six basins. The tracks are based on the IBTrACS dataset and the ERA5 reanalysis data from 1950 to 2023.

SST to TC PI increase, we followed the extreme weather sensitivity analysis[42,43] and employed a physical diagnostic approach to decompose V_m sensitivity into three variables, e.g.,ΔT_o, ΔT_s and $\Delta(\ln\theta_e^* - \ln\theta_e)$. The TC PI can be expressed as:

$$V_m = \sqrt{c_p(T_s - T_0)\frac{T_s}{T_0}\frac{C_k}{C_d}(\ln\theta_e^* - \ln\theta_e)|_m} \tag{10}$$

Let F represent the expression under the square root:

$$F = c_p(T_s - T_0)\frac{T_s}{T_0}\frac{C_k}{C_d}(\ln\theta_e^* - \ln\theta_e)|_m \tag{11}$$

The sensitivity of V_m to each variable X_i is calculated using partial derivatives:

$$\frac{\partial V_m}{\partial X_i} = \frac{1}{2\sqrt{F}}\frac{\partial F}{\partial X_i} \tag{12}$$

For TC outflow temperature (T_0):

$$\frac{\partial F}{\partial T_0} = c_p\frac{C_k}{C_d}\ln\frac{\theta_e^*}{\theta_e}\left(-\frac{T_s^2}{T_0^2}\right) \tag{13}$$

For TC underlying SST (T_s):

$$\frac{\partial F}{\partial T_s} = c_p\frac{C_k}{C_d}\ln\frac{\theta_e^*}{\theta_e}\left(\frac{2T_s}{T_0} - 1\right) \tag{14}$$

For humidity factor $(\ln\theta_e^* - \ln\theta_e)$:

$$\frac{\partial F}{\partial(\ln\theta_e^* - \ln\theta_e)} = c_p(T_s - T_0)\frac{T_s}{T_0}\frac{C_k}{C_d} \tag{15}$$

We calculate linear trends for three variables (T_0, T_s, $\ln\theta_e^* - \ln\theta_e$) over the 1950-2023 using least squares regression:

$$T_0(t) = a_{T_0}t + b_{T_0} \tag{16}$$

$$T_s(t) = a_{T_s}t + b_{T_s} \tag{17}$$

$$(\ln\theta_e^* - \ln\theta_e)(t) = a_{\ln\theta_e^* - \ln\theta_e}t + b_{(\ln\theta_e^* - \ln\theta_e)} \tag{18}$$

The variation of each variable was written as:

$$\Delta T_0 = a_{T_0}\Delta t \tag{19}$$

$$\Delta T_s = a_{T_s}\Delta t \tag{20}$$

$$\Delta(\ln\theta_e^* - \ln\theta_e) = a_{\ln\theta_e^* - \ln\theta_e}\Delta t \tag{21}$$

The PI change caused by each variable variation was calculated as:

$$\Delta V_{m,T_0} = \frac{\partial V_m}{\partial T_0}\Delta T_0 = \frac{1}{2\sqrt{F}}\frac{\partial F}{\partial T_0}a_{T_0}\Delta t \tag{22}$$

$$\Delta V_{m,T_s} = \frac{\partial V_m}{\partial T_s}\Delta T_s = \frac{1}{2\sqrt{F}}\frac{\partial F}{\partial T_s}a_{T_s}\Delta t \tag{23}$$

$$\Delta V_{m,\theta_e} = \frac{\partial V_m}{\partial(\ln\theta_e^* - \ln\theta_e)}\Delta(\ln\theta_e^* - \ln\theta_e) = \frac{1}{2\sqrt{F}}\frac{\partial F}{\partial(\ln\theta_e^* - \ln\theta_e)}a_{(\ln\theta_e^* - \ln\theta_e)}\Delta t \tag{24}$$

The contribution of each variable to TC PI can be expressed as:

$$\mathrm{Con}_{T_0} = \frac{\Delta V_{m,T_0}}{\Delta V_{m,T_0} + \Delta V_{m,T_s} + \Delta V_{m,\theta_e}} \tag{25}$$

$$\mathrm{Con}_{T_s} = \frac{\Delta V_{m,T_s}}{\Delta V_{m,T_0} + \Delta V_{m,T_s} + \Delta V_{m,\theta_e}} \tag{26}$$

$$\mathrm{Con}_{\theta_e} = \frac{\Delta V_{m,\theta_e}}{\Delta V_{m,T_0} + \Delta V_{m,T_s} + \Delta V_{m,\theta_e}} \tag{27}$$

The calculations were done combined equation (13-15), (22-24) and (25-27).

RESULTS

Global trends and contributing factors

Our analysis focused primarily on variations in TC outflow height during 1950–2023, based on 483,535 IBTrACS records from 8,478 TCs, including

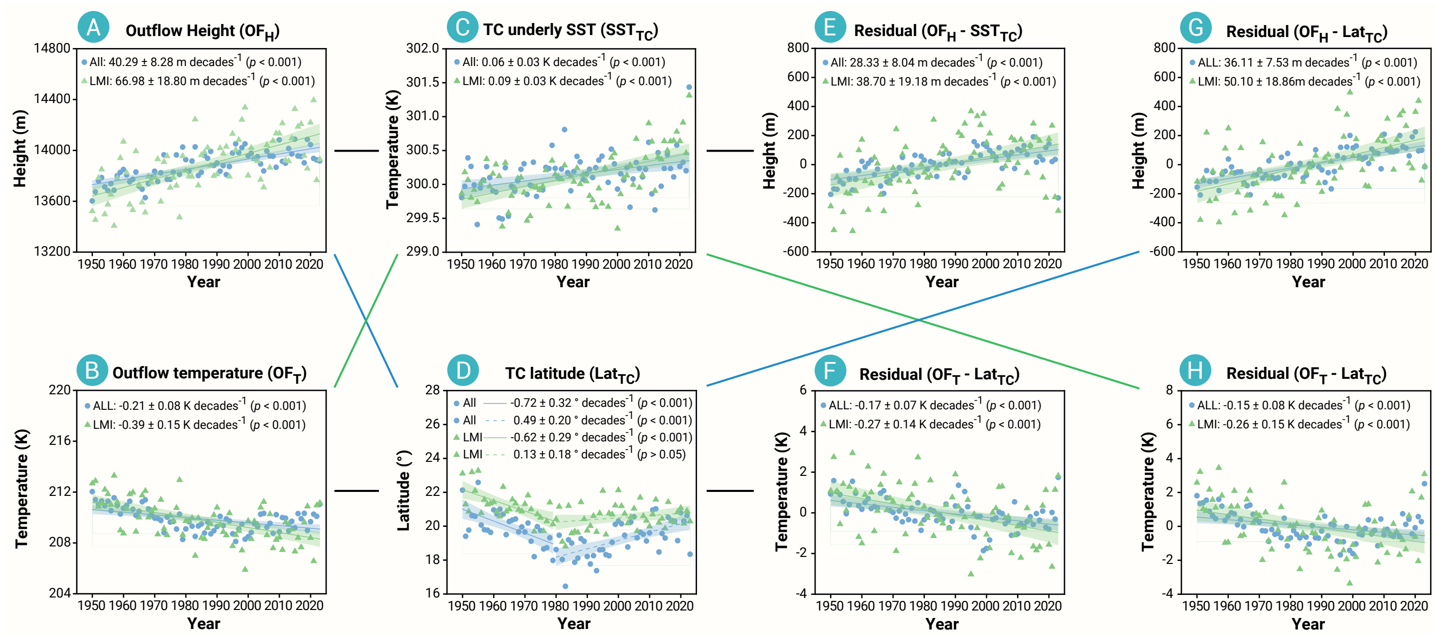

Figure 2. Temporal trends in TC outflow height and temperature from 1950 to 2023 (A) TC outflow height (OF_H; m) for the two records; (B) TC outflow temperature (OF_T; K); (C) TC underlying SST (SST_{TC}; K) within a 500 km radius of TC center; (D) TC center latitude (Lat_{TC}; °); (E) TC outflow height excluding the effect of TC underlying SST; (F) TC outflow height excluding the effect of TC latitude variations; (G) TC outflow temperature excluding the effect of TC underlying SST; (H) TC outflow temperature excluding the effect of TC latitude variations. Blue points and line represent All records; green points and line represent LMI records; linear trend lines are shown with their 95% two-sided confidence intervals (shaded). The colored connecting lines between panels illustrate the attribution pathways for the residual analysis (e.g., black lines connect OF_H to its residuals after excluding the effect of SST_{TC}).

systems from tropical depressions to super typhoons. The use of all such TC records provided a quantitative advantage in terms of sample size, and records of TC lifetime-maximum intensity (LMI) provided a qualitative advantage in data accuracy, as measurements taken around the time of LMI have much smaller uncertainties.[4] Accordingly, TC records were considered in terms of both "All records" and "LMI records". A significant increasing trend in TC outflow height was observed over the decades from 1950 to 2023 based on both All records (40.29 ± 8.28 m·decade^{-1}) and LMI records (66.98 ± 18.80 m·decade^{-1}) (Figure 2A).

In addition to observational and reanalysis data, we validated changes in the TC outflow environment using the Coupled Ocean–Atmosphere–Wave–Sediment Transport (COAWST) modeling system, which performs well in TC research.[44] To assess global warming effects, we configured three carbon emission scenarios (Historical, SSP245, and SSP585) using Coupled Model Intercomparison Project Phase 6 (CMIP6) data. TCs were implanted at locations of maximum genesis potential index (GPI; see Supporting Information text) under identical conditions, yielding 39 experiments across 13 groups (Figure S2). Details on the model configuration and the ideal TC initialization method are provided in Figure S3 and the Supporting Information text. In the model simulation results (Figure 3), the TC outflow height shows a clear upward trend with increasing carbon emissions (Historical: 13311 m, SSP245: 14,067 m, SSP585: 14,975 m), accompanied by a corresponding decrease in TC outflow temperature (Historical: 212.5 K, SSP245: 211.9 K, SSP585: 209.6 K), and is associated with an increase in TC potential intensity (Historical: 39.3 m·s^{-1}; SSP245: 42.7 m·s^{-1}; SSP585: 44.6 m·s^{-1}). These results are consistent with findings from observational and reanalysis datasets (Figures 2A-B).

Changes in TC outflow height result in part from changes in upper-atmosphere geopotential height in the six basins (Figure 1), which is projected to increase in response to global warming.[19] There is a statistically significant increase in the geopotential height of the TC outflow layer (300–100 hPa) over the 1950–2023 period. On a global scale, the increase in geopotential height ranges from 40 to 60 m for each pressure layer (Figure S4), notably less than totals of 294 m for All records and 496 m for LMI records (Figure 2A). The increase in geopotential height caused by global warming is therefore not the main factor contributing to the upward trend in TC outflow height.

SST is the primary energy source for TC genesis and intensification, so is also potentially an important factor determining TC activity (as well as TC outflow height) under global warming scenarios.[45] Our results indicate that TC underlying SST (SST within a 500 km radius of the TC center) becomes warmer over recent decades, for both All records and LMI records (Figure 2C), consistent with previous observations.[46] The increase in SST is likely to foster more robust vertical convection near TCs,[47] promoting an increase in outflow height (Figure S5). We excluded the contribution of ocean warming by regressing outflow height time series onto variability in TC underlying SST.[4] A marked decline in the rate of increase in outflow height was observed in both datasets, from 40.29 to 28.33 m·decade^{-1} for All records, and 66.98 to 38.70 m·decade^{-1} for LMI records (Figures 2A & E), underscoring the influence of TC underlying SST warming on the upward trend in TC outflow height.

The spatial location of TCs can influence their activity,[48] so the effect of spatial variation on TC outflow height must be considered. As the geopotential height of the upper-atmosphere generally decreases with latitude, TC outflow height (within the upper-atmosphere) is expected to be strongly influenced by variations in latitude. The vertically averaged geopotential height over 300–100 hPa (with TC outflow layers situated predominantly in these layers)[17,18] peaks in tropical latitudes and decreases progressively towards polar regions (Figure S6A), implying that changes in TC latitude may influence TC outflow height. The annual mean latitude of TCs has changed in recent decades. During 1950–1980, there was a pronounced equatorward shift in TC latitude (Figure 2D), possibly attributable to improvements in observational methodologies that enabled the detection of a greater number of weak TCs at lower latitudes.[20] Conversely, during 1981–2023, a notable poleward migration in TC latitude was observed (Figure 2D), possibly attributable to tropical expansion under global warming.[4] Note that, the significant increasing trend in TC outflow height was also observed over the decades from 1980 to 2023 based on both records (Figure S7) and the improvements in observational methodologies did not affect our main conclusions. To remove the effect of latitude variation, we regressed outflow height time series onto TC latitude variations (Figure 2E). A reduction in the upward outflow height trend was observed in both the All records (from 40.29 to 36.11 m·decade^{-1}) and LMI records (from 66.98 to 50.10 m·decade^{-1}). These findings suggest that TC latitude variations in response to global warming may influence the trend in TC outflow height. We also considered

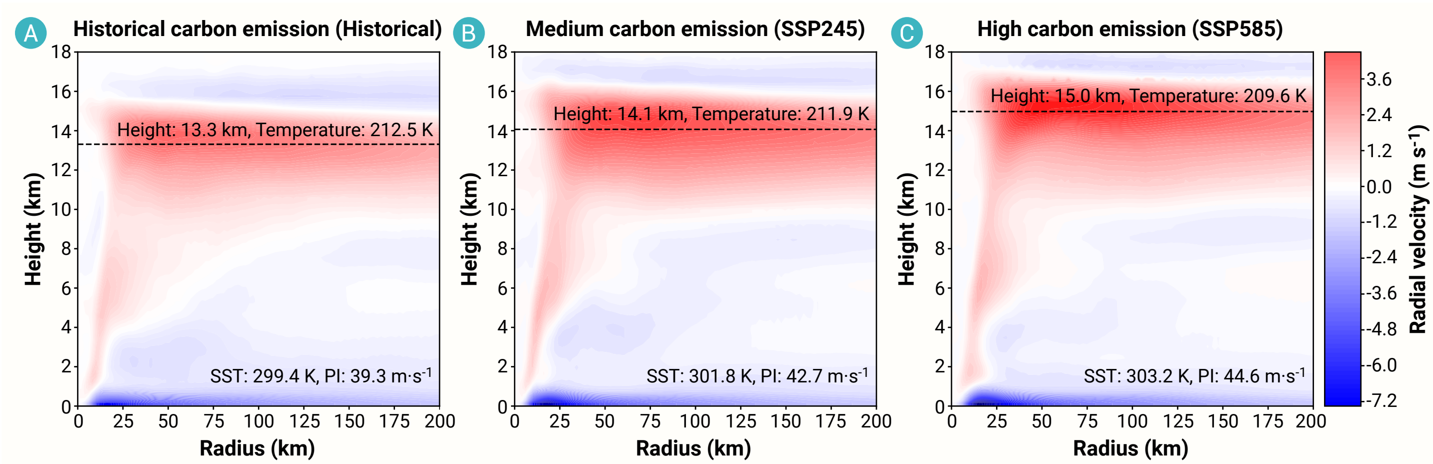

Figure 3. Azimuthal-averaged TC structures in the three carbon emission experiments (A) Historical carbon emission; (B) Medium carbon emission (SSP245); (C) High carbon emission (SSP585). Radial velocity (shading; m·s^{-1}), TC outflow height (m), TC outflow temperature (K), SST (K) and PI (m·s^{-1}).

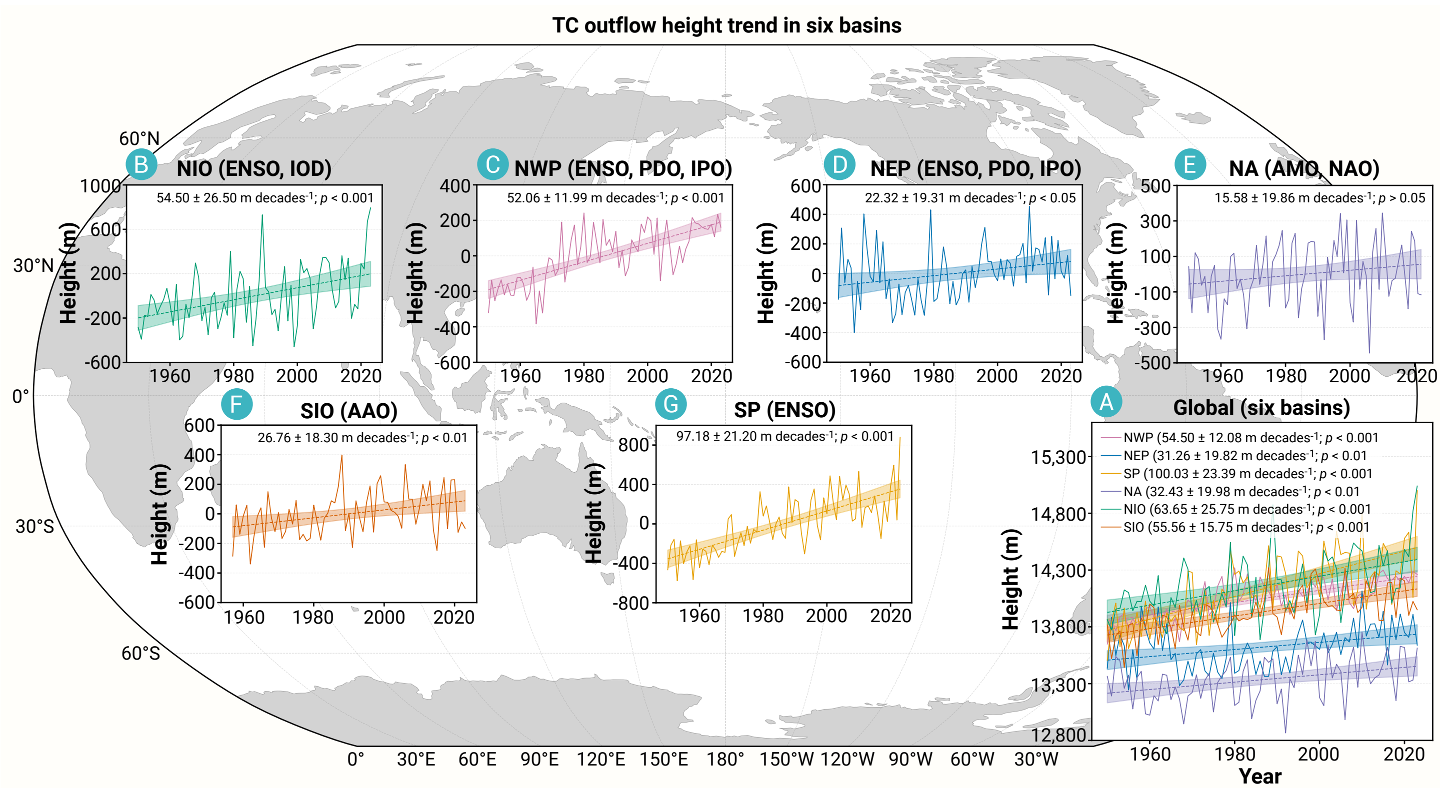

Figure 4. Temporal trends in TC outflow height from 1950 to 2023 Heights are shown for (A) the six basins; and excluding the effects of (B) the ENSO and IDO in the NIO; (C) the ENSO, PDO, and IPO in the NWP; (D) the ENSO, PDO, and IPO in the NEP; (E) the AMO and NAO in the NA; (F) the AAO in the SIO from 1957 to 2023 (for the AAO index from 1957) and (G) the ENSO in the SP. Color shading indicates 95% confidence intervals.

the possible effects in different basins in the next section.

To assess seasonal variations, we calculated the average TC outflow height for each season, with TCs occurring during March–May/June–August/September–November/December–February in the Northern Hemisphere and September–November/December–February/March–May/June–August in the Southern Hemisphere being categorized as spring/summer/autumn/winter TCs. Results indicate that the average TC outflow height is 13,945 m in spring, 13,923 m in summer, 13,825 m in autumn, and 14,062 m in winter, with TC outflow being slightly higher in spring and winter than in summer and autumn. Under global warming scenario, the seasonal variability in TC outflow height will likely contribute to the uptrend in TC outflow height, especially if the proportions of TCs in spring and winter increase. However, our analysis showed that the seasonal distribution of TCs has not changed significantly over recent decades (Figure S8), implying that the seasonal variability of TC outflow height has negligible influence on the upward trend.

Basin trends and natural variability

TC activity is influenced by a complex interplay of factors such as atmospheric circulation patterns, with specific regional characteristics,[48] and here we delineated TC activity regions into the six basins: the NWP, NEP, SP, NA, NIO, and SIO (Figure 1). Despite regional variations, the significant uptrends in TC outflow height are obvious across all basins, suggesting a pervasive global phenomenon (Figure 4A). The greatest uptrend occurs in the SP (100.03 ± 23.39 m·decade^{-1}), and the least in the NEP (31.26 ± 19.82 m·decade^{-1}), with intermediate values in the NWP (54.03 ± 12.08 m decade^{-1}), NA (32.43 ± 19.98 m·decade^{-1}), NIO (63.65 ± 25.75 m·decade^{-1}), and SIO (55.56 ± 15.75 m·decade^{-1}). The increase in TC outflow height is thus a global trend, and is still significant in all basins after removing the effect of latitude variations (Figure S9).

TC activity is influenced by natural variability, and the main influential natural variabilities vary among the basins. After the main influential natural variabili-

Table 1. Contribution of TC outflow height and upper-atmosphere temperature change to the reduction in TC outflow temperature.

Category	ΔH_{height} (m)	ΔT_{height} (°C)	$\Delta T_{upper_{atm}}$ (°C)	$\Delta T_{combine}$ (°C)	$\Delta T_{outflow}$ (°C)	E_{Pct} (%)
All records	267.23	-1.14	0.07	-1.08	-1.23	87%
LMI records	370.76	-1.58	0.10	-1.48	-1.98	75%
NWP	412.12	-1.81	0.07	-1.73	-2.11	82%
NEP	265.80	-1.09	0.39	-0.71	-0.48	69%
SP	738.74	-2.95	-0.02	-2.97	-4.30	69%
NA	154.09	-0.64	0.20	-0.44	-0.36	82%
NIO	493.35	-3.29	0.27	-3.02	-2.80	93%
SIO	414.53	-1.70	-0.26	-1.96	-2.18	90%

All records and LMI records were calculated using the mean vertical temperature gradient in all six basins, with specific basin calculations based on the vertical temperature gradient in that basin. ΔH_{height}, TC outflow height change; ΔT_{height}, TC outflow temperature change caused by the change of outflow height; ΔT_{upper_atm}, TC outflow temperature change caused by the change of upper-atmosphere temperature; $\Delta T_{combine}$, combined effects of ΔT_{height} and ΔT_{upper_atm}; $\Delta T_{outflow}$, TC outflow temperature change; E_P, explainable percentage.

Table 2. Contribution of TC outflow temperature and TC underlying SST change to TC PI change.

Category	ΔPI (m·s^{-1})	ΔPI caused by ΔT_o (m·s^{-1})	Con$_{T_0}$ (%)	ΔPI caused by ΔT_s (m·s^{-1})	Con$_{T_s}$ (%)	ΔPI caused by $\Delta(\ln\theta_e^* - \ln\theta_e)$ (m·s^{-1})	Con$_{\theta_e}$ (%)
All records	1.71	0.89	52%	0.22	13%	0.60	35%
LMI records	3.80	1.66	44%	0.36	9%	1.78	47%
NWP	3.80	1.11	29%	0.31	8%	2.38	63%
NEP	0.80	0.21	26%	0.32	41%	0.27	33%
SP	1.80	2.48	73%	0.11	3%	-0.79	24%
NA	1.99	0.60	30%	0.47	24%	0.92	46%
NIO	9.43	2.31	25%	0.45	5%	6.67	70%
SIO	-1.88	1.20	28%	0.01	1%	-3.09	71%

ΔPI, TC potential intensity change; ΔT_o, TC outflow temperature change; $\Delta(\ln\theta_e^* - \ln\theta_e)$, the change of the humidity effect in TC PI calculation, θ_e^* the saturation equivalent potential temperature at the ocean surface, and θ_e the boundary layer equivalent potential temperature; Con$_{T_0}$, contribution of TC outflow temperature change to TC PI increase; Con$_{T_s}$, contribution of TC underlying SST change to TC PI increase; Con$_{\theta_e}$, contribution of humidity effect change to TC PI increase.

ties in each basin eliminated (detail in the MATERIALS AND METHODS), the trend varied with different degrees among basins; e.g., decreased by ~50% in the NA and SIO, while increased by ~14% in the NIO, with little change in the NEP and SP (< 5%) (Figure 4). The trends of annual mean TC outflow height changed after removing the effect of natural variability, but were still significant in all basins. This indicates that, rather than natural variability, anthropogenic forcing is likely the main cause of the TC outflow height upward trends in the basins.

Relationship among TC outflow height, outflow temperature and potential intensity

Air temperature decreases with increasing height, so the TC outflow temperature decreases with increasing TC outflow height. Similar to TC outflow height, we investigated the observed trend in TC outflow temperature over the decades from 1950 to 2023, and found a significant decrease trend in TC outflow temperature based on both All records (-0.21 ± 0.09 K·decade^{-1}) and LMI records (-0.39 ± 0.17 K·decade^{-1}) (Figure 2B). We also investigated regional differences in TC outflow temperature changes across basins (Figure S10) and found that these temperature changes are generally consistent with the trend in TC outflow height, all of which passed the 95% significance test, except for NEP. This may be due to the warming of the tropospheric temperature in NEP, which is greatly influenced by SST.[49] Generally, the upper-atmosphere temperature changes consistently with the underlying SST.[50] We removed the effect of TC underlying SST to TC outflow temperature, with the downtrend decreased to 0.15 K·decade^{-1} for the All records and 0.26 K·decade^{-1} for the LMI records (Figure 2G). Like geopotential height, the upper-atmosphere temperature in the six basins also varies with latitude (Figure S6B). Elimination of the effects of latitude variations moderated the decrease in temperature in both records, with the downtrend decreasing to 0.17 K·decade^{-1} for the All records, and to 0.27 K·decade^{-1} for the LMI records (Figure 2H). This indicates that, similar to the important role of underlying SST and latitude to TC outflow height, they also contribute strongly to the trend in TC outflow temperature.

Notably, the increase in TC outflow height is not the only factor influencing TC outflow temperature, and the impact of upper-atmosphere temperature changes with global warming cannot be ignored. Generally, global warming causes upper-tropospheric temperatures (300–200 hPa) to increase, and lower-stratospheric temperatures (around 100 hPa) to decrease (Figure S4). The climatic warming effect is likely to have an impact on TC outflow temperature and should be considered for trends in TC outflow temperature. To further explore the reason for the downtrend in outflow temperature, we quantified the contribution of TC outflow height and upper-atmosphere

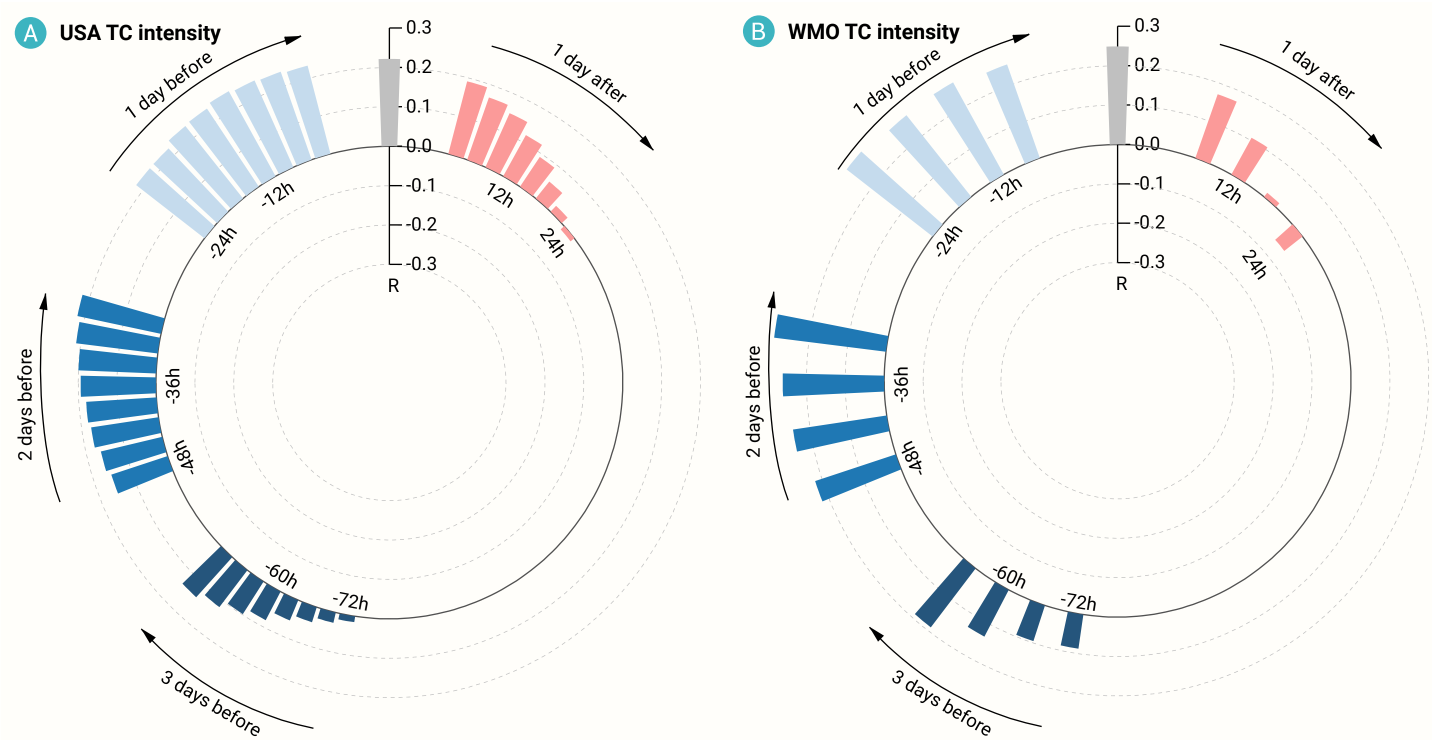

Figure 5. Correlation coefficients for antecedent and consequent variations in TC outflow height and TC intensity (A) TC intensity based on "USA_WIND" in IBTrACS dataset; and (B) TC intensity based on "WMO_WIND" in IBTrACS dataset. The term "1 day before (after)" indicates that TC outflow height (TC intensity) changes first, and TC intensity (TC outflow height) changes 1 day later, and so on. The calculation required the resequencing of TC time series, and the analysis was undertaken only when there were more than five time points remaining after resequencing. The resulting correlation had to pass a 95% confidence test.

temperature change to the reduction in TC outflow temperature (Table 1; calculation details in the MATERIALS AND METHODS section). The reduction in TC outflow temperature is primarily due to the combined effects of these two factors (explainable percentage > 69% in all categories, Table 1). Change of TC outflow height is likely the main control on the downtrend of TC outflow temperature, as the temperature change caused by the height change is similar to the total temperature change and much greater than that caused by the upper-atmosphere temperature change in all basins and records. The above results clearly indicate that TC outflow temperature decreases with increasing TC outflow height.

TC outflow temperature plays an important role in determining TC intensity.[16,17] Therefore, we consider TC outflow temperature as a "key bridge" connecting TC outflow height and TC intensity. Following the calculation method proposed by Emanuel et al.,[39-41] we evaluated the trends in TC PI under global warming, both globally and across basins (Figure S11). TC PI shows an overall increasing trend in most basins, with pronounced rises in the NWP and NIO, although some of these trends are not significant.

According to PI theory, both TC underlying SST and TC outflow temperature are important in determining TC PI (details in the Materials and Methods section). Generally, a more pronounced decrease in TC outflow temperature results in a higher TC PI.[51] We quantified the contributions of TC outflow temperature and underlying SST to the increase of PI, respectively (Table 2). On a global scale, the contribution of TC outflow temperature cooling to the increase in PI exceeds the direct contribution from TC underlying SST warming. Specifically, the SP exhibits the highest contribution from outflow temperature variations (73%), whereas the NIO records the lowest (25%). Note that, the contribution of SST warming to PI enhancement is likely underestimated, as SST also modulates PI via the humidity factor (thermodynamic disequilibrium), which is hard to quantify. This result indicates that the decrease in outflow temperature associated with the uptrend of TC outflow height substantially facilitates the intensification of TC PI.

To further clarify the causal relationship between TC outflow height and intensity, which can be compared to a chicken-and-egg problem, we performed a lead-lag correlation analysis. This approach allows us to examine both antecedent variations (outflow height changes preceding intensity) and consequent variations (intensity changes preceding outflow height). The results indicate that the maximum correlation occurs when the TC outflow height leads intensity by approximately 24 hours, which suggests that structural adjustments in the outflow layer likely act as a precursor to intensity variations (Figure 5). Such results are consistent with our finding that an increased outflow height induces a cooling of the outflow environment, thereby facilitating TC intensification. However, owing to the limited horizontal resolution of the data (0.25°), we were unable to clearly resolve the causal relationship from a dynamical perspective. To address this issue, we will involve the inversion of TC outflow height based on high-resolution observations (e.g. satellite, manned aircraft, dropsondes) to explore the relationship between TC outflow height and TC intensity more deeply from the perspective of dynamics in the future.

In summary, the significant upward trend of TC outflow height over the past few decades lead to a decrease in outflow temperature, and could indirectly benefit TC intensity.

DISCUSSION AND CONCLUSION

We quantified long-term historical global changes in TC outflow height using ERA5 reanalysis data and the IBTrACS dataset, and further validated this trend based on idealized numerical simulations. Our results indicate that over the past 74 years (1950–2023), the global TC outflow height has increased by 40.29 ± 8.28 m·decade^{-1}, with this upward trend being more pronounced in LMI records (66.98 ± 18.80 m·decade^{-1}; Figure 2A). The uptrend of TC outflow height is also statistically significant across all basins (Figure 4A). The strongest uptrend was observed in the SP, while the weakest was observed in the NEP. Uptrends in TC outflow height were still significant after removing the effects of natural variability, indicating that, rather than natural variability, anthropogenic forcing is likely the main cause of the outflow trends.

We attribute the increase in TC outflow height primarily to global warming, for the following reasons. (1) The geopotential height of the upper-atmosphere (300–100 hPa) has increased under global warming by 40–60 m over the past 74 years. This contributes to the increase in TC outflow height but is not the main cause, given that the total increase is ~300 m. (2) The TC underlying SST has increased significantly under global warming, enhancing vertical TC convection and further promoting an increase in TC outflow height. (3) We found that changes in TC latitude, which is proved to be associated with the global warming, also impact TC outflow height. When the effect of latitude variation is removed, the uptrend in TC outflow height for the LMI records decreases by almost 26%. The impacts of global warming differ across basins, potentially leading to regional difference in TC underlying SST, geopotential height, TC latitude, and so on. These factors further contribute to the spatial differences in TC outflow height trends. Owing to constraints in scope and manuscript length, a comprehensive investigation into the causes of these basin differences will be pursued in our future work.

Relative to TC air–sea interactions, changes in the TC outflow environment have received little attention. However, TC outflow environment has important influences on TC intensity, which is of great public concern. This study has found that, consistent with the uptrend in TC outflow height, there has been a concurrent downtrend in TC outflow temperature over recent decades. We consider that this reduction in temperature has been driven primarily by the increase in TC outflow height (93% in All records and 80% in LMI records). According to the Carnot cycle, a lower TC outflow temperature enhances the thermal gradient near TC, increasing TC PI. Globally, variations in TC outflow temperature account for 52% of the TC PI increase across the All records and 44% in LMI records. The effect of changes in TC outflow environment on TC intensity may be obscured by natural variability in short-term observations, but it could lead to a significant increase of TC intensity in the long-term future under global warming.

Our results suggest that the significant upward trend in outflow height under global warming leads to a decrease in outflow temperature, thereby exerting an indirect benefit on TC intensity. This trend, consistently identified in both historical observations and numerical experiments, highlights the robustness of the TC outflow environment's response to warming. While our simulations utilized the EC-Earth3 model to construct warming backgrounds, we acknowledge the potential for inter-model inconsistency among CMIP6 models.[52] Future research involving multi-model ensembles will be essential to further quantify these uncertainties and explore the mechanisms. Furthermore, due to current limitations in data resolution, the detailed dynamic causal relationship between TC outflow height and intensity remains a subject of ongoing investigation. Incorporating modern observational data (e.g., satellite, manned aircraft, and dropsondes) will help to describe the TC structure more clearly and resolve these uncertainties in the future.

REFERENCES

1. Emanuel K. (2005). Increasing destructiveness of tropical cyclones over the past 30 years. *Nature* **436**:686–688. DOI:10.1038/nature03906
2. Patricola C.M., Cassidy D.J. and Klotzbach P.J. (2022). Tropical oceanic influences on observed global tropical cyclone frequency. *Geophys. Res. Lett.* **49**:e2022GL099354. DOI:10.1029/2022GL099354
3. Huang P., Lin I.I., Chou C., et al. (2015). Change in ocean subsurface environment to suppress tropical cyclone intensification under global warming. *Nat. Commun.* **6**:7188. DOI:10.1038/ncomms8188
4. Kossin J.P., Emanuel K.A. and Vecchi G.A. (2014). The poleward migration of the location of tropical cyclone maximum intensity. *Nature* **509**:349–352. DOI:10.1038/nature13278
5. Xu J., Zhao P., Chan J.C.L., et al. (2024). Increasing tropical cyclone intensity in the western North Pacific partly driven by warming Tibetan Plateau. *Nat. Commun.* **15**:310. DOI:10.1038/s41467-023-44403-8
6. Peduzzi P., Chatenoux B., Dao H., et al. (2012). Global trends in tropical cyclone risk. *Nat. Clim. Change* **2**:289–294. DOI:10.1038/NCLIMATE1410
7. Bryan G.H. and Rotunno R. (2009). The maximum intensity of tropical cyclones in axisymmetric numerical model simulations. *Mon. Weather Rev.* **137**:1770–1789. DOI:10.1175/2008MWR2709.1
8. Camargo S.J. and Wing A.A. (2016). Tropical cyclones in climate models. *Wiley Interdiscip. Rev. Clim. Change* **7**:211–237. DOI:10.1002/wcc.373
9. Knutson T.R., Sirutis J.J., Garner S.T., et al. (2008). Simulated reduction in Atlantic hurricane frequency under twenty-first-century warming conditions. *Nat. Geosci.* **1**:359–364. DOI:10.1038/ngeo202
10. Sobel A.H., Camargo S.J., Hall T.M., et al. (2016). Human influence on tropical cyclone intensity. *Science* **353**:242–246. DOI:10.1126/science.aaf6574
11. Emanuel K.A. (1986). An air-sea interaction theory for tropical cyclones. *Part I: Steady-state maintenance. J. Atmos. Sci.* **43**:585–605. DOI:10.1175/1520-0469(1986)043<0585:AASITF>2.0.CO;2
12. Shimada U., Sawada M. and Yamada H. (2016). Evaluation of the accuracy and utility of tropical cyclone intensity estimation using single ground-based Doppler radar observations. *Mon. Weather Rev.* **144**:1823–1840. DOI:10.1175/MWR-D-15-0254.1
13. Emanuel K., Solomon S., Folini D., et al. (2013). Influence of tropical tropopause layer cooling on Atlantic hurricane activity. *J. Clim.* **26**:2288–2301. DOI:10.1175/JCLI-D-12-00242.1
14. Wing A.A., Emanuel K. and Solomon S. (2015). On the factors affecting trends and variability in tropical cyclone potential intensity. *Geophys. Res. Lett.* **42**:8669–8677. DOI:10.1002/2015GL066145
15. Trabing B.C., Bell M.M. and Brown B.R. (2019). Impacts of radiation and upper-tropospheric temperatures on tropical cyclone structure and intensity. *J. Atmos. Sci.* **76**:135–153. DOI:10.1175/JAS-D-18-0165.1
16. Emanuel K. and Rotunno R. (2011). Self-stratification of tropical cyclone outflow. Part I: Implications for storm structure. *J. Atmos. Sci.* **68**:2236–2249. DOI:10.1175/JAS-D-10-05024.1
17. Komaromi W.A. and Doyle J.D. (2017). Tropical cyclone outflow and warm core structure as revealed by HS3 dropsonde data. *Mon. Weather Rev.* **145**:1339–1359. DOI:10.1175/MWR-D-16-0172.1
18. Merrill R.T. and Velden C.S. (1996). A three-dimensional analysis of the outflow layer of Supertyphoon Flo (1990). *Mon. Weather Rev.* **124**:47–63. DOI:10.1175/1520-0493(1996)124<0047:ATDAOT>2.0.CO;2
19. He C. and Zhou W. (2020). Different enhancement of the East Asian summer monsoon under global warming and interglacial epochs simulated by CMIP6 models: Role of the subtropical high. *J. Clim.* **33**:9721–9733. DOI:10.1175/JCLI-D-20-0304.1
20. Knapp K.R., Kruk M.C., Levinson D.H., et al. (2010). The international best track archive for climate stewardship (IBTrACS) unifying tropical cyclone data. *Bull. Am. Meteorol. Soc.* **91**:363–376. DOI:10.1175/2009BAMS2755.1
21. Hersbach H., Bell B., Berrisford P., et al. (2020). The ERA5 global reanalysis. *Q. J. R. Meteorol. Soc.* **146**:1999–2049. DOI:10.1002/qj.3803
22. Nakamura R. and Mäll M. (2021). Pseudo global warming sensitivity experiments of subtropical cyclone Anita (2010) under RCP 8.5 scenario. *J. Geophys. Res. Atmos.* **126**:e2021JD035261. DOI:10.1029/2021JD035261
23. Vidale P.L., Hodges K., Vannière B., et al. (2021). Impact of stochastic physics and model resolution on the simulation of tropical cyclones in climate GCMs. *J. Clim.* **34**:4315–4341. DOI:10.1175/JCLI-D-20-0507.1
24. Sun Y., Zhong Z., Li T., et al. (2017). Impact of ocean warming on tropical cyclone track over the western North Pacific: A numerical investigation based on two case studies. *J. Geophys. Res. Atmos.* **122**:8617–8630. DOI:10.1002/2017JD026959
25. Neu U., Akperov M.G., Bellenbaum N., et al. (2013). A community effort to intercompare extratropical cyclone detection and tracking algorithms: Assessing method-related uncertainties. *Bull. Am. Meteorol. Soc.* **94**:529–547. DOI:10.1175/BAMS-D-11-00154.1
26. Shi J., Feng X., Toumi R., et al. (2024). Global increase in tropical cyclone ocean surface waves. *Nat. Commun.* **15**:174. DOI:10.1038/s41467-023-43532-4
27. Hodges K., Cobb A. and Vidale P.L. (2017). How well are tropical cyclones represented in reanalysis datasets. *J. Clim.* **30**:5243–5264. DOI:10.1175/JCLI-D-16-0557.1
28. Chen B.F., Davis C.A. and Kuo Y.H. (2021). Examination of the combined effect of deep-layer vertical shear direction and lower-tropospheric mean flow on tropical cyclone intensity and size based on the ERA5 reanalysis. *Mon. Weather Rev.* **149**:4057–4076. DOI:10.1175/MWR-D-21-0120.1
29. Klotzbach P.J. and Oliver E.C.J. (2015). Variations in global tropical cyclone activity and the Madden-Julian Oscillation since the midtwentieth century. *Geophys. Res. Lett.* **42**:4199–4207. DOI:10.1002/2015GL063966
30. Camargo S.J., Robertson A.W., Gaffney S.J., et al. (2007). Cluster analysis of typhoon tracks. Part II: Large-scale circulation and ENSO. *J. Clim.* **20**:3654–3676. DOI:10.1175/JCLI4203.1
31. Li S., Mei W. and Xie S.P. (2022). Effects of tropical sea surface temperature variability on Northern Hemisphere tropical cyclone genesis. *J. Clim.* **35**:4719–4739. DOI:10.1175/JCLI-D-21-0084.1
32. Patricola C.M., Cassidy D.J. and Klotzbach P.J. (2022). Tropical oceanic influences on observed global tropical cyclone frequency. *Geophys. Res. Lett.* **49**:e2022GL099354. DOI:10.1029/2022GL099354
33. Mazza E. and Chen S.S. (2023). Modulation of tropical cyclone tracks and rainfall by the North Atlantic Oscillation. *J. Geophys. Res. Atmos.* **128**:e2022JD038107. DOI:10.1029/2022JD038107
34. Klotzbach P.J. and Gray W.M. (2008). Multidecadal variability in North Atlantic tropical cyclone activity. *J. Clim.* **21**:3929–3935. DOI:10.1175/2008JCLI2162.1
35. Saji N.H., Goswami B.N., Vinayachandran P.N., et al. (1999). A dipole mode in the tropical Indian Ocean. *Nature* **401**:360–363. DOI:10.1038/43854
36. Xie S.P., Hu K., Hafner J., et al. (2009). Indian Ocean capacitor effect on Indo-western Pacific climate during the summer following El Niño. *J. Clim.* **22**:730–747. DOI:10.1175/2008JCLI2544.1
37. Park C.H., Choi J., Son S.W., et al. (2023). Sub-seasonal variability of ENSO teleconnections in Western North America and its prediction skill. *J. Geophys. Res. Atmos.* **128**:e2022JD037985. DOI:10.1029/2022JD037985

38. Mao R., Gong D.Y., Yang J., et al. (2013). Is there a linkage between the tropical cyclone activity in the southern Indian Ocean and the Antarctic Oscillation. *J. Geophys. Res. Atmos.* 118:8519–8535. DOI:10.1002/jgrd.50666
39. Emanuel K.A. (1995). Sensitivity of tropical cyclones to surface exchange coefficients and a revised steady-state model incorporating eye dynamics. *J. Atmos. Sci.* 52:3969–3976. DOI:10.1175/1520-0469(1995)052<3969:SOTCTS>2.0.CO;2
40. Bister M. and Emanuel K.A. (2002). Low frequency variability of tropical cyclone potential intensity 2. Climatology for 1982–1995. *J. Geophys. Res. Atmos.* 107:ACL 5-1-4. DOI:10.1029/2001JD000780
41. Bister M. and Emanuel K.A. (2002). Low frequency variability of tropical cyclone potential intensity 1. Interannual to interdecadal variability. *J. Geophys. Res. Atmos.* 107:ACL 26-1-15. DOI:10.1029/2001JD000776
42. Gu L., Yin J., Gentine P., et al. (2023). Large anomalies in future extreme precipitation sensitivity driven by atmospheric dynamics. *Nat. Commun.* 14:3197. DOI:10.1038/s41467-023-39039-7
43. Norris J., Chen G. and Neelin J.D. (2019). Thermodynamic versus dynamic controls on extreme precipitation in a warming climate from the community Earth system model large ensemble. *J. Clim.* 32:1025–1045. DOI:10.1175/JCLI-D-18-0302.1
44. Shi L., Olabarrieta M., Nolan D.S., et al. (2020). Tropical cyclone rainbands can trigger meteotsunamis. *Nat. Commun.* 11:678. DOI:10.1038/s41467-020-14423-9
45. Bell M.M. and Montgomery M.T. (2008). Observed structure, evolution, and potential intensity of category 5 Hurricane Isabel (2003) from 12 to 14 September. *Mon. Weather Rev.* 136:2023–2046. DOI:10.1175/2007MWR1858.1
46. Kieu C., Zhao M., Tan Z., et al. (2023). On the role of sea surface temperature in the clustering of global tropical cyclone formation. *J. Clim.* 36:3145–3162. DOI:10.1175/JCLI-D-22-0623.1
47. Yu J. and Wang Y. (2009). Response of tropical cyclone potential intensity over the north Indian Ocean to global warming. *Geophys. Res. Lett.* 36:L03709. DOI:10.1029/2008GL036742
48. Klotzbach P.J. and Oliver E.C.J. (2015). Variations in global tropical cyclone activity and the Madden-Julian Oscillation since the midtwentieth century. *Geophys. Res. Lett.* 42:4199–4207. DOI:10.1002/2015GL063966
49. Done J.M., Lackmann G.M. and Prein A.F. (2022). The response of tropical cyclone intensity to changes in environmental temperature. *Weather Clim. Dyn.* 3:693–711. DOI:10.5194/wcd-3-693-2022
50. Vecchi G.A. and Soden B.J. (2007). Effect of remote sea surface temperature change on tropical cyclone potential intensity. *Nature* 450:1066–1070. DOI:10.1038/nature06423
51. Vecchi G.A., Fueglistaler S., Held I.M., et al. (2013). Impacts of atmospheric temperature trends on tropical cyclone activity. *J. Clim.* 26:3877–3891. DOI:10.1175/JCLI-D-12-00503.1
52. Guan S., Huang M., Cai W., et al. (2026). Weak self-induced cooling of tropical cyclones amid fast sea surface warming. *Nat. Geosci.* 19:153–158. DOI:10.1038/s41561-025-01879-x

FUNDING AND ACKNOWLEDGMENTS

This work was sponsored by the National Natural Science Foundation of China (Grants 42075035 and 42075011). The funders had no role in study design, data collection and analysis, decision to publish, or preparation of the manuscript.

AUTHOR CONTRIBUTIONS

The research was designed by Y. S. and Z. F., with analysis of the results conducted by both authors. Calculation method was performed by Z. F., Y. S., W. Zhong., and H. Z., who also wrote the initial draft of the manuscript. Z. F., Y. Liang., and Z. B. made visualization. Y. S., W. Zhong., H. Z. and W. Zhang. contributed to writing-editing. Z. F. and Y. S. contributed data curation. All authors contributed to the manuscript and approved the final version.

DECLARATION OF INTERESTS

The authors declare no competing interests.

DATA AND CODE AVAILABILITY

TC position revise and outflow calculation was done based on ERA5 reanalysis data at https://cds.climate.copernicus.eu/datasets/reanalysis-era5-pressure-levels?tab=download and https://cds.climate.copernicus.eu/datasets/reanalysis-era5-single-levels?tab=download (last access: 1 March 2026). Natural variability is available for download at https://psl.noaa.gov/data/correlation/ (last access: 1 March 2026). The CMIP6 data are available for download at https://aims2.llnl.gov/search/cmip6/ (last access: 1 March 2026). The COAWST model is available for download at https://www.usgs.gov/centers/whcmsc/science/coawst-a-coupled-ocean-atmosphere-wave-sediment-transport-modeling-system (last access: 1 March 2026). All data are available in the main text or the supplementary materials.

SUPPLEMENTAL INFORMATION

It can be found online at https://doi.org/10.59717/j.xinn-geo.2026.100248.